Colombo, C. and McInnes, C.R. (2010) Orbit design for future SpaceChip swarm missions. In: 61st Aeronautical Congress, IAC 2010, 27 September - 1 October 2010, Prague, Czech Republic.

ORBIT DESIGN FOR FUTURE SPACECHIP SWARM MISSIONS

Camilla Colombo
Advanced Space Concepts Laboratory, University of Strathclyde, Glasgow, United Kingdom
camilla.colombo@strath.ac.uk

Colin R. McInnes
Advanced Space Concepts Laboratory, University of Strathclyde, Glasgow, United Kingdom
colin.mcinnes@strath.ac.uk

The effect of solar radiation pressure and atmospheric drag on the orbital dynamics of satellites-on-a-chip (SpaceChips) is exploited to design long-lived orbits about the Earth. The orbit energy gain due to asymmetric solar radiation pressure, considering the Earth shadow, is used to balance the energy loss due to atmospheric drag. Future missions for a swarm of SpaceChips are proposed, where a number of small devices are released from a conventional spacecraft to perform spatially distributed measurements of the conditions in the ionosphere and exosphere. It is shown that the orbit lifetime can be extended and indeed selected through solar radiation pressure and the end-of-life re-entry of the swarm can be ensured, by exploiting atmospheric drag.

I. INTRODUCTION

Recent innovations in spacecraft design exploit advances in miniaturisation to fabricate small satellites with dimensions of a single chip (1 cm × 1 cm × 25 μm [1]). In addition, current concepts for MEMS (micro-electromechanical systems) devices have been designed with micro-power sources, sensing, computing and bi-directional communication capabilities for terrestrial 1 mm^3 'smart dust' applications [2-3]. These existing capabilities have also been exploited to design near-term concepts for functional devices in space, such as satellite-on-a-chip (SpaceChip) [4-7].

This new technology offers the benefit of low-cost manufacturing of vast numbers of micro-spacecraft (e.g., up to 10,000) for use in swarm applications. The considerably smaller dimensions of satellites-on-a-chip envisage their deployment in orbit from a CubeSat or as piggy-back on a conventional spacecraft, thus allowing significant launch cost savings.

The deployment of vast numbers of SpaceChips will enable future missions, such as global sensor networks for Earth observation and communication, distributed space missions for multi-point, real-time sensing for space science (space weather, geomagnetic physics, reflectometry), interplanetary exploration in support of traditional spacecraft, or deployment in the vicinity of a spacecraft for diagnostic or environmental detection purposes.

As an early example of a SpaceChip-scale swarm, project West Ford in 1963 placed a ring of 4.8×10^8 copper dipole antennas (1.78 cm long needles, with a diameter of 17.8 μm) into orbit to allow global radio communication [8]. The motion of the individual dipoles, from dispensing to final re-entry through the atmosphere was both modelled and observed. More recently, Petschek et al. [9] proposed a Kilo-Satellite constellation mission (less than one kilogram satellites) for the distributed measurement of the global instantaneous structure of the magnetosphere.

The realisation of these swarm concepts requires an understanding of orbital dynamics at extremely small spacecraft length-scales. The significantly higher area-to-mass ratio of future SpaceChip or smaller 'smart dust' devices, with respect to conventional spacecraft, requires new insights into orbital dynamics, as perturbations such as solar radiation pressure (SRP) and aerodynamic drag become dominant with respect to the Earth's gravity.

In Ref. [10] the orbital dynamics of such 'smart dust' devices was analysed and the energy input from asymmetric solar radiation pressure was used to offset the energy dissipation of atmospheric drag, without the use of active control. Families of long-lived orbits for swarms of SpaceChips where presented for which the condition of Sun-synchronous apse-line precession is achieved passively without any propellant mass consumption. A comparison with the drag-only and SRP-only scenarios shown that the exploitation of the natural effects of solar radiation pressure and atmospheric drag provides a means of enabling long-lived orbits for future SpaceChip and 'smart dust' devices without the use of active control and ensures the final re-entry of the devices so that they do not constitute future space debris. Due to the large area-to-mass ratio of these devices orbit lifetime due to air drag alone is extremely short.

In this paper the natural effects of solar radiation pressure and atmospheric drag perturbations are

exploited to design swarms missions for the mapping and study of the upper regions of the Earth's atmosphere. A swarm of SpaceChips is proposed as distributed nodes of a network to obtain a spatial and temporal map of the ionosphere and exosphere.

Given the initial orbital elements of the spacecraft, the shadow geometry is determined as a function of semi-major axis, eccentricity and angular displacement between the Sun-Earth line and the orbit pericentre. The secular change of the in-plane orbital elements over a single orbit revolution is evaluated analytically in the presence of Earth shadow. The coupled effect of atmospheric drag and solar radiation pressure, with asymmetry due to eclipses, is exploited to greatly extend the orbit lifetime of such devices and to assess and design the disposal of the devices at the end of the mission. Importantly, the short lifetime of high area-to-mass spacecraft can be greatly extended (and indeed selected) through the interaction of energy gain from asymmetric solar radiation pressure and energy dissipation due to drag.

The paper is organised as follows: Section II introduces the analytical approach to compute the orbit evolution; Section III presents the conditions for long-lived orbits and summarises the results for partial equilibrium orbits and their long-term behaviour under the effect of solar radiation pressure and drag. In Section IV the effect of natural perturbations is exploited to design swarm missions for the study of the upper stages of the Earth's atmosphere.

II. ORBITAL DYNAMICS

The orbit evolution of the spacecraft is obtained through an averaging technique with Gauss' planetary equations to obtain the secular variation of the orbital elements. As a first approach to explore orbital dynamics at extremely small length-scales, we consider only solar radiation pressure and the atmospheric drag, whose perturbing accelerations are proportional to the area-to-mass ratio of the spacecraft; hence their effect is dominant for small devices. Again, to begin to explore conditions for long-lived orbits we constrain the present study to orbits lying in the ecliptic plane.

II.I. Solar radiation pressure

We consider a spacecraft on an Earth-centred orbit lying in the ecliptic plane as represented in Fig. 1. The satellite is subjected to an acceleration due to solar radiation pressure given by

$$a_{r,\,\mathrm{SRP}} = a_{\mathrm{SRP}} \cos(\omega - \lambda_{\mathrm{Sun}})$$
$$a_{\theta,\,\mathrm{SRP}} = -a_{\mathrm{SRP}} \sin(\omega - \lambda_{\mathrm{Sun}})$$
(1)

where a_r and a_θ are the components of the acceleration along the radial and transverse direction in

the orbital plane, and a_{SRP} is the characteristic acceleration

$$a_{\mathrm{SRP}} = \frac{p_{\mathrm{SR}} c_R A_\odot}{m}$$
(2)

where $p_{\mathrm{SR}} = 4.56 \times 10^{-6} \, \dfrac{\mathrm{N}}{\mathrm{m}^2}$ is the solar pressure at 1 AU, c_{R} the reflectivity coefficient, $A_\odot$ is the area exposed to the Sun, and m is the mass of the satellite. The angle $\omega - \lambda_{\mathrm{Sun}}$ represents the angular displacement between the orbit pericentre (ω) and the Sun-line direction λ_{Sun}.

Fig. 1   Orbit geometry.

The effect of SRP on the spacecraft orbit is expressed in terms of long-term variation of the orbital elements. Gauss' equations for the variation of semi-major axis a, eccentricity e and anomaly of the pericentre are given by [11]

$$\frac{da}{df} = \frac{2pr^2}{\mu_{\mathrm{Earth}}\left(1-e^2\right)^2}\left(e\sin f \cdot a_r + \frac{p}{r}\cdot a_\theta\right)$$

$$\frac{de}{df} = \frac{r^2}{\mu_{\mathrm{Earth}}}\left(\sin f \cdot a_r + \left(1+\frac{r}{p}\right)\cos f \cdot a_\theta + e\frac{r}{p}\cdot a_\theta\right)$$
(3)

$$\frac{d\omega}{df} = \frac{r^2}{\mu_{\mathrm{Earth}}e}\left(-\cos f \cdot a_r + \left(1+\frac{r}{p}\right)\sin f \cdot a_\theta\right)$$

with μ_{Earth}, the gravitational parameter of the Earth, r the orbit radius, and p the semilatus rectum. These are integrated in true anomaly f, considering the other orbital elements to be constant over one orbit revolution. In the case of a constant disturbing acceleration in a fixed inertial direction defined in Eq. (1), Gauss' equations can be solved in closed form to

find the primitive functions f_a, f_e, f_ω for semi-major axis, eccentricity and anomaly of the pericentre:

$$f_a\left(a,\,e,\,\omega-\lambda_{\text{Sun}}\right)=\int\frac{da}{df}df+c_a$$

$$f_e\left(a,\,e,\,\omega-\lambda_{\text{Sun}}\right)=\int\frac{de}{df}df+c_e \qquad (4)$$

$$f_\omega\left(a,\,e,\,\omega-\lambda_{\text{Sun}}\right)=\int\frac{d\omega}{df}df+c_\omega$$

Some integration constants c_a, c_e and c_ω are introduced in the primitive functions but they are removed when the primitive function is evaluated at two limits of integration. Substituting Eq. (1) in Eqs. (3) the indefinite integrals can be computed, as shown in Eqs. (4). After some algebraic manipulations we obtain:

$$f_a=-\frac{2a^3\left(1-e^2\right)}{\mu_{\text{Earth}}}a_{\text{SRP}}\frac{1}{e\left(1+e\cos f\right)}\left(\cos\left(\omega-\lambda_{\text{Sun}}\right)+\right.$$
$$\left.+e\sin\left(\omega-\lambda_{\text{Sun}}\right)\sin f\right)+c_a$$

$$f_e=\frac{a^2\left(1-e^2\right)^2}{\mu_{\text{Earth}}}a_{\text{SRP}}\left(\sin\left(\omega-\lambda_{\text{Sun}}\right)\left(-\frac{3}{2}\frac{E}{\left(1-e^2\right)^{3/2}}+\right.\right.$$
$$\left.+\frac{\sin f\left(\cos f\left(-8e^4+10e^2-2\right)+6e\left(1-e^2\right)\right)}{4\left(1-e^2\right)^2\left(1+e\cos f\right)^2}\right)+$$
$$\left.-\frac{\cos\left(\omega-\lambda_{\text{Sun}}\right)}{2e^2\left(1+e\cos f\right)^2}\left(1+2e\cos f+e^2\right)\right)+c_e$$

$$f_\omega=-\frac{a^2\left(1-e^2\right)^2}{\mu_{\text{Earth}}e}a_{\text{SRP}}\left(\cos\left(\omega-\lambda_{\text{Sun}}\right)\left(\frac{3}{2}\frac{E}{\left(1-e^2\right)^{3/2}}+\right.\right.$$
$$\left.-\frac{e\sin f}{\left(1-e^2\right)\left(1+e\cos f\right)}-\frac{1}{2}\frac{\left(e+\cos f\right)\sin f}{\left(1-e^2\right)\left(1+e\cos f\right)^2}\right)+$$
$$\left.+\sin\left(\omega-\lambda_{\text{Sun}}\right)\frac{1+2e\cos f}{2e^2\left(1+e\cos f\right)^2}\right)+c_\omega$$
$$(5)$$

where E is the eccentric anomaly which is a function of the true anomaly. Note that Eqs. (5) have been obtained under the assumption that the orbit lies in the ecliptic plane. Eqs. (5) assumes that the disturbing acceleration a_{SRP} is constant when the spacecraft is in sunlight, i.e., the variation of the solar flux over time is neglected, and the exposed area $A_\odot$ in Eq. (2) is considered constant (i.e., the spacecraft has a spherical shape or the attitude of the spacecraft is kept constant with respect to the Sun-line). At this point, the total variation of the orbital

elements can be evaluated over the orbit arc in which the spacecraft is in sunlight: $\left[0,\,f_{\text{ecl, enter}}\right],\left[f_{\text{ecl, exit}},\,2\pi\right]$, which is function of a, e, $\omega-\lambda_{\text{Sun}}$ at the orbit pericentre and the true anomaly at which the satellite enters and exits the eclipses, $f_{\text{ecl, enter}}$ and $f_{\text{ecl, exit}}$. Since we are assuming the orbital elements and a_{SRP} to be fixed over one orbit revolution, at their value at the pericentre, the total variation of the orbital elements can be written as:

$$\Delta a_{\text{SRP, }2\pi}\left(a,\,e,\,\omega-\lambda_{\text{Sun}},\,f_{\text{ecl, exit}},\,f_{\text{ecl, enter}}\right)=\left[f_a\right]_{f_{\text{ecl, exit}}}^{f_{\text{ecl, enter}}}$$

$$\Delta e_{\text{SRP, }2\pi}\left(a,\,e,\,\omega-\lambda_{\text{Sun}},\,f_{\text{ecl, exit}},\,f_{\text{ecl, enter}}\right)=\left[f_e\right]_{f_{\text{ecl, exit}}}^{f_{\text{ecl, enter}}} \quad (6)$$

$$\Delta\omega_{\text{SRP, }2\pi}\left(a,\,e,\,\omega-\lambda_{\text{Sun}},\,f_{\text{ecl, exit}},\,f_{\text{ecl, enter}}\right)=\left[f_\omega\right]_{f_{\text{ecl, exit}}}^{f_{\text{ecl, enter}}}$$

In the planar case we consider (i.e., the orbit lies in the ecliptic plane), and assuming that the parallax of the Sun is negligible, the arguments of true anomaly at which the satellite enters and exits the Earth's shadow are given by the following systems (see Fig. 1):

$$f_{\text{ecl, exit}}\left(a,e,\omega-\lambda_{\text{Sun}}\right):\begin{cases}r\cos\left(\omega-\lambda_{\text{Sun}}+f\right)>0\\ r\sin\left(\omega-\lambda_{\text{Sun}}+f\right)=+R_{\text{E}}\end{cases}$$
$$f_{\text{ecl, enter}}\left(a,e,\omega-\lambda_{\text{Sun}}\right):\begin{cases}r\cos\left(\omega-\lambda_{\text{Sun}}+f\right)>0\\ r\sin\left(\omega-\lambda_{\text{Sun}}+f\right)=-R_{\text{E}}\end{cases} \quad (7)$$

where R_{E} is the mean radius of the Earth, and r the orbital radius. The expressions for $f_{\text{ecl, exit}}\left(a,e,\omega-\lambda_{\text{Sun}}\right)$ and $f_{\text{ecl, enter}}\left(a,e,\omega-\lambda_{\text{Sun}}\right)$ can be expressed as a closed-form function of the orbital elements a, e, and $\omega-\lambda_{\text{Sun}}$ [10]. The expressions for $f_{\text{ecl, exit}}\left(a,e,\omega-\lambda_{\text{Sun}}\right)$ and $f_{\text{ecl, enter}}\left(a,e,\omega-\lambda_{\text{Sun}}\right)$ can be substituted into Eqs. (6) to give the actual variation of orbital elements considering the Earth's shadow. If the spacecraft does not enter into eclipse, $f_{\text{ecl, enter}}=f_{\text{ecl, exit}}+2\pi$, some terms of Eqs. (6) vanish (the terms containing $\sin f$ and $\cos f$), in particular the variation of semi-major axis vanishes. In the case of no eclipse, Eqs. (6) simplify to the formulation used by McInnes et al. [12] and Oyama et al. [13].

The secular and long-period rate of change of the orbital elements can be obtained by dividing Eqs. (6) by the Keplerian orbital period

$$T=2\pi\sqrt{\frac{a^3}{\mu_{\text{Earth}}}} \qquad (8)$$

thus giving

$$\frac{d\overline{a}}{dt}\bigg|_{\text{SRP}}=\frac{\Delta a_{\text{SRP, }2\pi}}{2\pi}\sqrt{\frac{\mu_{\text{Earth}}}{a^3}} \qquad (9a)$$

$$\frac{d\overline{e}}{dt}\bigg|_{\text{SRP}} = \frac{\Delta e_{\text{SRP, }2\pi}}{2\pi}\sqrt{\frac{\mu_{\text{Earth}}}{a^3}} \qquad (9b)$$

$$\frac{d\overline{\omega}}{dt}\bigg|_{\text{SRP}} = \frac{\Delta \omega_{\text{SRP, }2\pi}}{2\pi}\sqrt{\frac{\mu_{\text{Earth}}}{a^3}} \qquad (9c)$$

where the superscript dash is used to indicate the secular variation. The line of apsides of the ellipse will rotate due to the perturbing solar radiation pressure acceleration, with a mean rate of precession given by the Eq. (9c) that can be rewritten to express the perigee precession with respect to the Sun-line, introducing the orbital rate of the Earth around the Sun $n_{\text{Earth-Sun}}$ so that

$$\frac{d\left(\overline{\omega}-\overline{\lambda}_{\text{Sun}}\right)}{dt}\bigg|_{\text{SRP}} = \frac{\Delta \omega_{\text{SRP, }2\pi}}{2\pi}\sqrt{\frac{\mu_{\text{Earth}}}{a^3}} - n_{\text{Earth-Sun}}$$

II.II. Atmospheric drag

For spacecraft orbits with a low perigee the motion is also influenced by atmospheric drag acceleration

$$\mathbf{a}_{\text{Drag}} = -\frac{1}{2}\frac{c_D A_{\text{Drag}}}{m}\rho v_{rel}^2 \hat{\mathbf{v}}_{rel} \qquad (10)$$

where c_D is the drag coefficient, A_{Drag} is the effective cross-sectional area of the spacecraft and m its mass, v_{rel} is the velocity relative to the rotating atmosphere and $\hat{\mathbf{v}}_{rel}$ the corresponding unit vector. The secular disturbing effect on the orbit due to atmospheric drag can be modelled analogously to the case of solar radiation pressure. Starting from Gauss' equations written as function of the eccentric anomaly, King-Hele [14] derived equations which express the secular perturbation on the orbital elements due to atmospheric drag. These equations are based on the assumption of a time-independent, spherically-symmetric atmosphere with a density that varies exponentially with altitude h, according to:

$$\rho = \rho_0 \exp\left[-\frac{h-h_0}{H}\right] \qquad (11)$$

where ρ_0 is the reference density at the reference altitude h_0 and H is the scale height, whose values are taken from tables [15]. If we neglect atmospheric rotation (i.e., the angular velocity of the Earth ω_{Earth} is zero), the variation of $\Delta\omega_{\text{Drag, }2\pi}$ due to drag is zero, while the change of the in-plane orbital elements over a single revolution is given by [16]:

$$\Delta e_{\text{Drag, }2\pi} = -2\pi\delta a\rho_p \exp[-c]\left\{I_1 + \frac{e}{2}\left(I_0 + I_2\right)\right.$$

$$\left. -\frac{e^2}{8}\left(5I_1 - I_3\right) - \frac{e^3}{16}\left(5I_0 + 4I_2 - I_4\right) + O\left(e^4\right)\right\}$$

$$\Delta h_{p\text{ Drag, }2\pi} = -2\pi\delta a^2\rho_p \exp[-c]\left\{\left(I_0 - I_1\right)\right.$$

$$-\frac{e}{2}\left(3I_0 - 4I_1 + I_2\right) + \frac{e^2}{8}\left(6I_0 - 11I_1 + 6I_2 - I_3\right) +$$

$$\left. -\frac{e^3}{16}\left(7I_0 - 12I_1 + 8I_2 - 4I_3 + I_4\right) + O\left(e^4\right)\right\}$$

$$\Delta a_{\text{Drag, }2\pi} = \frac{\Delta h_{p\text{ Drag, }2\pi} + a\cdot\Delta e_{\text{Drag, }2\pi}}{1-e}$$

$$\Delta\omega_{\text{Drag, }2\pi} = 0$$

$$(12)$$

where ρ_p is the density at the orbit perigee, computed through Eq. (11), the factor $c = \dfrac{ae}{H}$, I_k are the modified Bessel functions of the first kind of order k and argument c [17], and $\delta = \dfrac{QA_{\text{drag}}c_D}{m}$ (where the drag coefficient c_D is considered constant, and the factor Q is equal to 1 for static atmosphere). Note that Eqs. (12) are valid up to the order of eccentricity indicated, within the range $0.01 \le e \le 0.8$.

In Ref. [10] the validity of Eqs. (6) and Eqs. (12) was verified by comparison with the numerical integration of the dynamics in Cartesian coordinates, using the expression for the disturbing accelerations Eq. (1) and Eq. (10).

Analogously to Eqs. (9), we obtain the secular and long-period rate of change of the orbital elements by dividing Eqs. (12) by the Keplerian orbital period:

$$\frac{d\overline{a}}{dt}\bigg|_{\text{Drag}} = \frac{\Delta a_{\text{Drag, }2\pi}}{2\pi}\sqrt{\frac{\mu_{\text{Earth}}}{a^3}}$$

$$\frac{d\overline{e}}{dt}\bigg|_{\text{Drag}} = \frac{\Delta e_{\text{Drag, }2\pi}}{2\pi}\sqrt{\frac{\mu_{\text{Earth}}}{a^3}} \qquad (13)$$

$$\frac{d\overline{\omega}}{dt}\bigg|_{\text{Drag}} = 0$$

The total secular variation of the orbital elements can be expressed as:

$$\frac{d\bar{a}}{dt} = \frac{d\bar{a}}{dt}\bigg|_{\text{SRP}} + \frac{d\bar{a}}{dt}\bigg|_{\text{Drag}}$$

$$\frac{d\bar{e}}{dt} = \frac{d\bar{e}}{dt}\bigg|_{\text{SRP}} + \frac{d\bar{e}}{dt}\bigg|_{\text{Drag}} \qquad (14)$$

$$\frac{d\bar{\omega}}{dt} = \frac{d\bar{\omega}}{dt}\bigg|_{\text{SRP}}$$

III. LONG-LIVED ORBITS

In Ref. [10] the conditions for long-lived orbits for 'smart dust' devices with solar radiation pressure and atmospheric drag were defined in the orbit phase-space, and numerical integration of the secular variation of orbital elements Eq. (14) was used to characterise the long-term evolution of those orbits. In the following section the method to determine equilibrium and partial equilibrium orbits will be summarised and an overview of long-lived orbits for SpaceChips will be given. A detailed analysis of the orbital element change due to solar radiation pressure and drag and a characterisation of families for long-lived orbits is given in Ref. [10].

III.I. Conditions for long-lived orbits

To study the effect on the satellite's orbit of the influence of both solar radiation pressure and atmospheric drag, the secular variation of the Keplerian elements over a single orbital revolution can be computed by adding Eqs. (6) to Eqs. (12), under the assumption that the coupling between SRP and atmospheric drag is negligible to first order.

The search for equilibrium orbits imposes three conditions to be satisfied. The total variation of semi-major axis and eccentricity due to SPR and drag must be zero, i.e., the combined effect of the two natural perturbations must cancel. Moreover, the Sun-synchronous condition imposes the requirement that the change in argument of perigee over one orbit due to SRP (recall from Eqs. (12) that $\Delta\omega_{\text{Drag},2\pi} = 0$) must be equal to the angular displacement of the Earth around the Sun (i.e., the apparent motion of the Sun around an Earth inertial system) over one orbital period of the spacecraft, such that the net change of ω is zero.

$$\begin{cases} \Delta a_{\text{SRP},2\pi} + \Delta a_{\text{Drag},2\pi} = 0 & \text{(a)} \\ \Delta e_{\text{SRP},2\pi} + \Delta e_{\text{Drag},2\pi} = 0 & \text{(b)} \\ \Delta\omega_{\text{SRP},2\pi} = \Delta\lambda_{\text{Sun},2\pi} & \text{(c)} \end{cases} \qquad (15)$$

with $\Delta\lambda_{\text{Sun},2\pi} = n_{\text{Earth-Sun}} \cdot T$, T being the orbital period, given by Eq. (8). Note that Eq. (15c) in the simplified case without Earth shadow was adopted by McInnes et al. [12] and Oyama et al. [13] for determining the required characteristic acceleration of a solar sail to provide Sun-synchronous apse-line precession.

An analysis of the change in orbital elements due to solar radiation pressure and atmospheric drag as a function of the initial conditions of the satellite (i.e., the values of the Keplerian elements a, e, and $\omega - \lambda_{\text{Sun}}$ at the orbit pericentre) was performed [10]. From the study of the sign of $\Delta a_{\text{SRP},2\pi}$, $\Delta a_{\text{Drag},2\pi}$, $\Delta e_{\text{SRP},2\pi}$, $\Delta e_{\text{Drag},2\pi}$, $\Delta\omega_{\text{SRP},2\pi}$ and $\Delta\lambda_{\text{Sun},2\pi}$ it is possible to define the domain of angular displacements $\omega - \lambda_{\text{Sun}}$ where each of the equations of system Eq. (15) can be satisfied.

- The total change in semi-major axis Eq. (15a) can be zero within the range $0 \le \omega - \lambda_{\text{Sun}} \le \pi$ (the limit values are for the case of SRP only).
- The total variation of eccentricity Eq. (15b) can be zero for $\pi \le \omega - \lambda_{\text{Sun}} \le 2\pi$ (the limit values are for the case of SRP only).
- The Sun-synchronous condition Eq. (15c) can be solved for $\pi/2 \le \omega - \lambda_{\text{Sun}} \le 3\pi/2$ (the limit values are for a circular orbit).

Therefore, system Eq. (15) cannot be satisfied if both solar radiation pressure and atmospheric drag are present. If the effect of drag is negligible, equilibrium orbits can be identified under the effect of solar radiation pressure for $\omega - \lambda_{\text{Sun}} = \pi$. When solar radiation pressure and atmospheric drag both have a non-negligible effect on the spacecraft orbit, even if a complete equilibrium is not possible, it is useful to study *partial equilibrium* solutions:

$$\begin{cases} \Delta a_{\text{SRP},2\pi} + \Delta a_{\text{Drag},2\pi} = 0 \\ \Delta\omega_{\text{SRP},2\pi} = \Delta\lambda_{\text{Sun},2\pi} \end{cases} \qquad (16)$$

$$\begin{cases} \Delta e_{\text{SRP},2\pi} + \Delta e_{\text{Drag},2\pi} = 0 \\ \Delta\omega_{\text{SRP},2\pi} = \Delta\lambda_{\text{Sun},2\pi} \end{cases} \qquad (17)$$

in which the Sun-synchronous condition is satisfied and only one variation, either semi-major axis or eccentricity is zero.

The solution of Eqs. (15)–(17), which identify the initial conditions for equilibrium or partial equilibrium orbits can be numerically computed through a global multi-start approach. A local algorithm is started from several points randomly distributed over the entire domain of semi-major axis, eccentricity and argument of angular displacement $\omega - \lambda_{\text{Sun}}$. The numerical solution is made possible by the use of the semi-analytical approach explained in Section II. Alternatively, the use of full numerical simulation for determining the change in orbital elements over a single orbit and the numerical solution of the eclipse geometry would make the computational time for the solution of systems Eqs. (15)–(17) impractical. Starting from each point on the mesh, a local minimisation is performed

numerically [18-19]. The objective function used for the minimisation is:

$$\min_{\{a,\, e,\, \omega-\lambda_{\text{Sun}}\}} \Big[w_a \left| \Delta a_{\text{Drag},\, 2\pi} + \Delta a_{\text{SRP},\, 2\pi} \right| +$$

$$+ w_e \left| \Delta e_{\text{Drag},\, 2\pi} + \Delta e_{\text{SRP},\, 2\pi} \right| +$$

$$+ w_\omega \left| \Delta \omega_{\text{SRP},\, 2\pi} - \Delta \lambda_{\text{Sun},\, 2\pi} \right| \Big]$$

where w_a, w_e, w_ω are weight parameters introduced to treat this multi-objective minimisation problem (the three equations of Eqs. (15) must be solved) as a single-objective minimisation. Depending on the value of the weight parameters, the multi-start algorithm can identify the solution set of system Eq. (15), Eq. (16), or Eq. (17). The ratio between w_a and w_ω, and w_e and w_ω were chosen such that, for any solution found the Sun-synchronous apse-line condition is always satisfied. We restricted the eccentricity to be within the range $0.01 \leq e \leq 0.8$ which is of practical interest.

III.II. Results for partial equilibrium orbits

The solution of the systems Eqs. (15)-(17) can be represented in the phase space $\{ e \quad \omega - \lambda_{\text{Sun}} \quad h_p \}$ or equivalently $\{ e \quad \omega - \lambda_{\text{Sun}} \quad a \}$, as depicted in Fig. 2. The characteristics of the SpaceChip used for estimating the Keplerian element change due to SRP and drag are reported in Section IV.I.

The red surface is the solution of the Sun-synchronous condition $\Delta \omega_{\text{SRP},\, 2\pi} = \Delta \lambda_{\text{Sun},\, 2\pi}$, while the magenta surface on the domain $\pi \leq \omega - \lambda_{\text{Sun}} \leq 2\pi$ contains the initial conditions for which the variation of the eccentricity due to SRP and drag balances (i.e., $\Delta e_{\text{SRP},\, 2\pi} + \Delta e_{\text{Drag},\, 2\pi} = 0$) and the blue surface on the domain $0 \leq \omega - \lambda_{\text{Sun}} \leq \pi$ represents the solution of $\Delta a_{\text{SRP},\, 2\pi} + \Delta a_{\text{Drag},\, 2\pi} = 0$.

For an eccentricity higher than approximately 0.115 and perigee height above 900 km, a set of solutions for system Eq. (15) exists with the condition $\omega - \lambda_{\text{Sun}} = \pi$ (i.e., the three surfaces intersect in correspondence of the black line C). With these initial conditions the orbit perigee is along the Sun–Earth direction, facing the Sun. This position is a stable condition for the variation of $\omega - \lambda_{\text{Sun}}$ and the change in eccentricity and semi-major axis over one orbit cancels, as the effect or SRP is symmetric in this configuration, and the drag is negligible (over one orbit); hence the orbit precesses due to SRP alone. Considering the branch of the graph with $\omega - \lambda_{\text{Sun}} = \pi$, the greater the decrease of perigee height and eccentricity, the greater the effect of drag becomes up to a certain point at which it cannot be neglected. Beyond this point, as expected from the analysis in section III.I, no global equilibrium solutions

(Eq. (15)) can be found. In this region (for perigee heights below 800 km approximately), atmospheric drag and SRP have comparable effects. However, a set of solutions still exist for system Eq. (16) (i.e., $\Delta a_{2\pi} = 0$ and sun-synchronous condition satisfied) and Eq. (17) (i.e., $\Delta e_{2\pi} = 0$ and Sun-synchronous condition satisfied), represented respectively by the black branches A and B of the graph. Note that each point in Fig. 2 corresponds to an initial condition for an Earth-centred orbit. Fig. 2 is therefore an example of a bifurcation. A solution for global equilibrium orbits (system Eq. (15)) can be found for eccentricities and perigee heights higher than a certain value (bifurcation point). Below the bifurcation point, the equilibria disappear and the only possible solution degrades to system Eq. (16) or Eq. (17) (only two out of the three equations of system Eq. (15) can be satisfied).
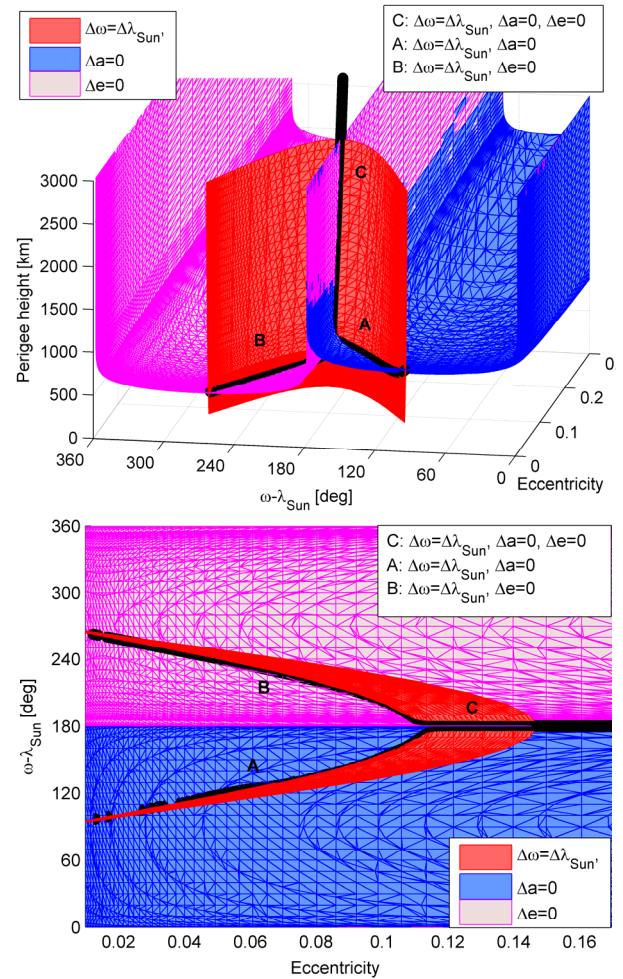

Fig. 2:   Long-lived orbits conditions for the SpaceChip whose characteristics are reported in Section IV.I. Surfaces representing each of the equations of system Eq. (15). a) 3D view, and b) 2D view in eccentricity$-\left(\omega - \lambda_{\text{Sun}} \right)$.

Fig. 3 shows the contour lines of the variation of orbital elements for two fixed values of $\omega - \lambda_{\text{Sun}}$. For $\omega - \lambda_{\text{Sun}} = 160\,\text{deg}$ (Fig. 3a) the partial equilibrium solution, represented by the black dot, is in correspondence of Eq. (16) satisfied, but the total variation of $\Delta e_{2\pi}$ 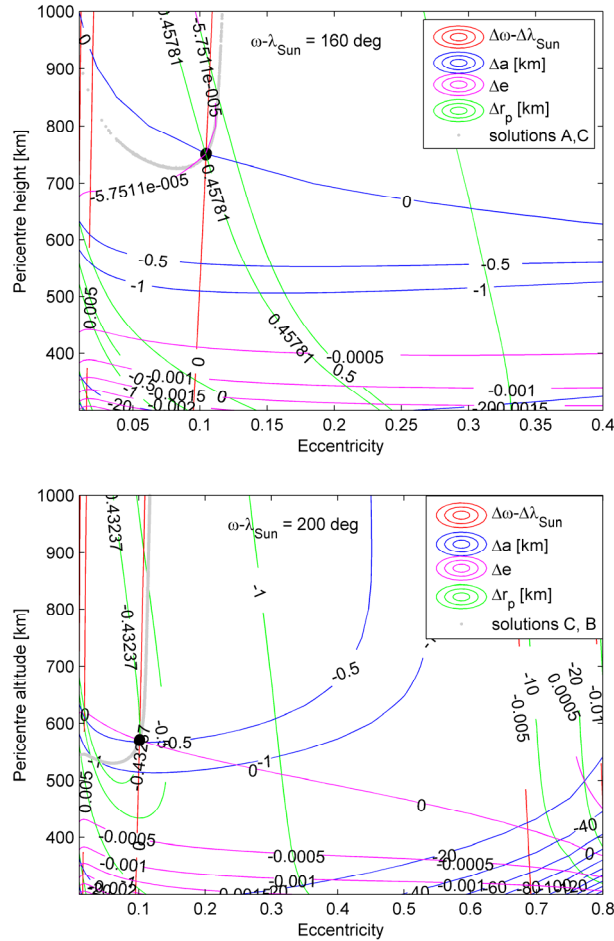is negative and the change in perigee height is positive. For $\omega - \lambda_{\text{Sun}} = 200\,\text{deg}$ (Fig. 3b), instead, the partial equilibrium solution, represented by the black dot, is in correspondence of Eq. (17) satisfied, but the total variation of $\Delta a_{2\pi}$ is negative and the change in perigee height is negative.

Fig. 3: Contour lines of the change of orbital elements in correspondence of the solution for log-lived orbits. a) Solution for $\omega - \lambda_{\text{Sun}} = 160\,\text{deg}$, and b) solution for $\omega - \lambda_{\text{Sun}} = 200\,\text{deg}$.

III.III. Long-term orbit evolution

The long-term evolution of orbits whose initial conditions are represented by the set of points in Fig. 2 was analysed in [10]. The long-term behaviour can be predicted by integrating Eqs. (14) and using a stopping condition for the integration.

Different families of long-lived orbits were presented [10]. In those regions of the phase-space where the effect of atmospheric drag is negligible, equilibrium orbits can be found under the effect of solar radiation pressure only. These solutions correspond to points belonging to branch C of the surface graph in Fig. 2, with an initial perigee altitude over a minimum value.

If the initial condition is in a certain region around the equilibrium solution set, the long-term evolution is characterised by *librational motion, progressively decaying* due to the non-conservative effect of atmospheric drag. It is possible to define different arcs of the orbit evolution where the trajectory is dominated either by drag or by solar radiation pressure. Asymmetry in solar radiation pressure due to eclipses leads to modulation of the orbit energy and angular momentum, and families of orbits can be found where the energy gain due to radiation pressure balances the energy dissipation due to drag.

In addition, the effect of atmospheric drag can be exploited to ensure the end-of-life decay of SpaceChips, thus preventing long-lived orbit debris.

IV. SPACECHIP SWARM MISSIONS

The employment of MEMS devices for space applications offer significant potential, mainly due to low cost of fabrication and launch or deployment as piggy-back on a conventional spacecraft. Therefore, it is possible to identify new space missions addressing goals that cannot be met with larger systems.

Firstly, such devices can be deployed in a swarm for real time applications, to collect measurements on a spatially distributed domain. Their ideal application is for taking single measurements (temperature, detect the presence or absence or a particular pre-defined condition, etc.) rather than performing complex analysis on each single device [1]. Moreover, their disposability enables mission designs with high risk, since a lost device can be easily replaced, and the average behaviour of the swarm can be studied, rather than the evolution of each satellite[1] [4, 8-9].

Swarms of SpaceChips can enable new missions, such as remote sensing for Earth observation, space weather, reflectometry and interferometry (oceanic properties such as surface height, significant wave height, wind speed and wind direction), spectrometry, and even more challenging missions for interplanetary and deep space exploration, in support of conventional spacecraft.

---

[1] ChipSat workshop, 18 February 2010, Brown University, website: http://www.engin.brown.edu/ chipsat/index.html [retrieved on 07 September 2010].

In Ref. [10] it was shown that the Sun-synchronous apse-line precession can be artificially obtained with a SpaceChip corresponding to current nano-fabrication technologies. This concept can be adapted to enhance the return of a GEOSAIL type mission [12-13]. A swarm of SpaceChips can be used as distributed nodes of a network in the useful region of the phase-space, to obtain a spatial and temporal map of the geomagnetic tail, similar to the concept of the Kilo-Satellite constellation proposed by Petschek et al. [9].

In this paper we propose the employment of a SpaceChip swarm for mapping the upper stages of the atmosphere. In particular the ionosphere extends from approximately 80 km to 640 km; in this region the gases which compose the Earth's atmosphere are rarefied, the atoms are ionised by solar radiation and the level of ionisation is highly influenced by solar activity. An understanding of this area would be particularly interesting as conditions in the ionosphere influence the quality of transmission from communication satellites[2].

At higher altitudes (up to approximately 1280 km) the low-density region of the Earth's atmosphere extends to the exosphere, where atoms and molecules escape, due to exchange of electrical charges between the solar wind and the outer parts of the Earth's atmosphere[3].

IV.I. Spacecraft and perturbation model

We consider a silicon microchip (density 2.3 g/cm^3) of 1×1 cm^2 and 0.025 mm thick. This was taken from the design by Atchison and Peck [1], hence it represents a near-term device. Table 1 reports the SpaceChip dimensions and the radius of a spherical particle with an equivalent area-to-mass ratio. The sphere shape is usually adopted for studies on interplanetary dust [20]. Since the SpaceChip density is assumed uniform, the characteristic length is represented by the chip's thickness:

$$A_{\text{chip}} = l_1^2 \qquad \frac{A}{m} = \frac{1}{l_2 \cdot \rho_{\text{silicon}}}$$
$$m_{\text{chip}} = l_1^2 \cdot l_2 \cdot \rho_{\text{silicon}}$$

where A is the cross-section area.

In this paper we consider that the average effective cross-section $A_\odot$ exposed to the Sun is always equal to the cross-sectional area of the spacecraft A. This implies that the spacecraft has a spherical shape or its attitude is kept fixed with respect to the Sun-line. A passive Sun-pointing attitude control was proposed for millimeter-scale solar sails, based on faceted surfaces to stabilise a

Sun-pointing plate [1]. Alternately, electro-chromic elements with variable reflectance can be layered at the sides of the chip to be exploited as a steering device, as tested on the IKAROS mission [21]. Moreover, a reflectivity coefficient $c_R = 1.8$ is assumed (note that for a black body $c_R = 1$, for a flat mirror perpendicular to the light direction $c_R = 2$).

For the model of atmospheric drag, a drag coefficient $c_D = 2.1$ is chosen ($c_D = 2.2$ is usually used for a flat plate model, $c_D = 2.0$ to 2.1 for spherical particles), and the cross-sectional area A_{Drag} is considered constant and equal to the cross-sectional area of the spacecraft. The reference values for the computation of the air density in Eq. (11) where taken equal as [15]:

$$h_0 = 600 \text{ km}$$
$$\rho_0 = 1.454 \times 10^{-13} \text{ kg/m}^3$$
$$H = 71.835 \text{ km}$$

since the region where solar radiation pressure and atmospheric drag are known to have comparable effect is approximately around 400–800 km. A more accurate value of the density would be obtained by selecting the reference values h_0, ρ_0 and H closest to the range of orbit altitudes considered. Table 1 also contains the characteristic acceleration due to solar radiation pressure computed through Eq. (2).

Table 1: SpaceChip characteristics.

Parameter	Value
Chip dimensions [mm]	$10 \times 10 \times 0.025$
Sphere dimensions [mm]	0.0187
A/m [m^2/kg]	17.39
a_{SRP} [mm/s^2]	0.1427

The long-term evolution of the SpaceChips is predicted by integrating Eqs. (14) until the perigee altitude decreases below $h_p \leq 50$ km. This is set because below a certain perigee altitude the orbit rapidly decays and the mission is terminated. The numerical integration was performed through an adaptive step-size Runge-Kutta-Fehlberg integration scheme integrator with a six stage pair of approximation of the fourth and fifth order [22], with absolute and relative tolerance of 2.5×10^{-14}.

---

[2] http://science.nasa.gov/missions/terriers/ [retrieved on 07 September 2010].
[3] http://www.ibex.swri.edu/ [retrieved on 07 September 2010].

IV.II. Mission for mapping the upper layers of the atmosphere

A larger, conventional spacecraft whose design is reported in Table 2 is injected into an Earth orbit lying in the ecliptic plane, with initial eccentricity 0.15 and pericentre height of 450 km. The spacecraft motion will be only marginally influenced by solar radiation pressure and atmospheric drag, therefore its orbit will follow for some time a quasi-vertical line in the eccentricity–$(\omega - \lambda_{Sun})$ phase space (i.e., the orbit apse-line drifts with respect to the Sun-Earth line with a period of one year).

Table 2: Carrier spacecraft characteristics.

Parameter	Value
m	100 kg
A	0.8 m^2
c_D	2.1
c_R	1.2

As this dispenser spacecraft moves on its orbit, it will release a number of SpaceChips. The period of the year in which the 'smart dust' devices are released is chosen such that $\pi/2 < \omega_{s/c} - \lambda_{Sun} < \pi$ (i.e., the orbit perigee is in sunlight and the condition $\Delta a_{SRP+Drag} > 0$ is satisfied [10]). Because of their high area-to-mass, the SpaceChip devices will not follow the carrier orbit; rather their orbit will evolve under the effect of solar radiation pressure and drag, as described in Section III.III and [10]. Fig. 4 represents the phase-space coverage of the SpaceChip mission over one year. The red line corresponds to the orbit of the dispenser spacecraft; over one year it traces a full vertical line in the domain $\omega - \lambda_{Sun}$. In correspondence to each black dot, a number of SpaceChips can be released from the carrier. The long-term evolution of the SpaceChips orbits is shown with the blue line. For the first part of the orbit evolution for $\omega - \lambda_{Sun} < \pi$, $\Delta a_{SRP+Drag} > 0$ and $\Delta e_{SRP+Drag} < 0$; as a consequence the orbit perigee rises reaching its maximum at $\omega - \lambda_{Sun} = \pi$. Afterwards, when $\omega - \lambda_{Sun} > \pi$, $\Delta a_{SRP+Drag} < 0$ and $\Delta e_{SRP+Drag} > 0$, hence the perigee height decreases. At a zone below 600 km, the influence of drag becomes predominant and causes the following decay of the SpaceChip orbits (the blue dot indicates an altitude below 50 km). The effect of perigee altitude fluctuation is more pronounced as the argument of perigee of the release orbit moves far from $\omega_{s/c} - \lambda_{Sun} = \pi$.

The argument of orbit perigee drifts following the apparent Sun-line rotation, starting behind the Sun for $\omega - \lambda_{Sun} < \pi$ and moving ahead for $\omega - \lambda_{Sun} > \pi$. We denote this kind of orbit evolution as a *librational* orbit. In Fig. 4 the orbit evolution under the effect of drag only is superimposed (green line), starting from the same initial conditions identified by the black dots. The orbit shrinks while the radius of the perigee tends to remain constant (see also Fig. 10).
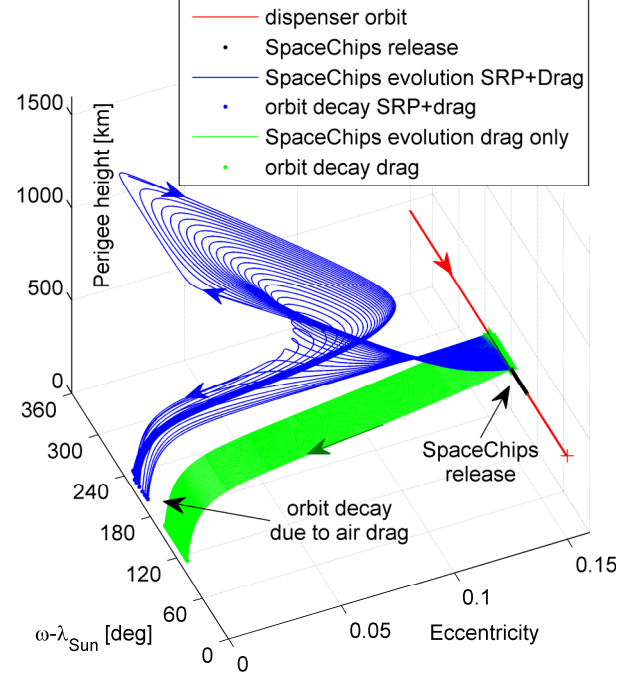
Fig. 4: SpaceChip swarm evolution in the phase-space. The dispenser spacecraft follows the red orbit; the long-term evolution of the released chips under the effect of SRP and drag is represented by the blue line. The evolution under the effect of drag only is represented with the green line.

Fig. 5 shows an example of the evolution of a *librational and progressively decaying* SpaceChip orbit (any blue line in Fig. 4) in an Earth centred reference frame, with its *x*-axis rotating with the Sun-line direction. The long-term behaviour of the orbit perigee is described by the blue line. Note the initial SpaceChip orbit, which is equal to the dispenser orbit (green orbit), and the final decay phase, when the perigee quickly decreases. The orbit perigee is always in sunlight, allowing communication when the 'smart dust' devices pass closer to the Earth surface, or with a carrier spacecraft.
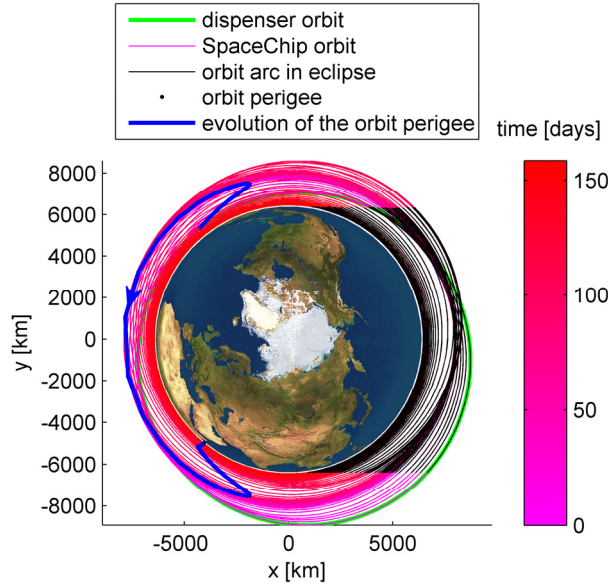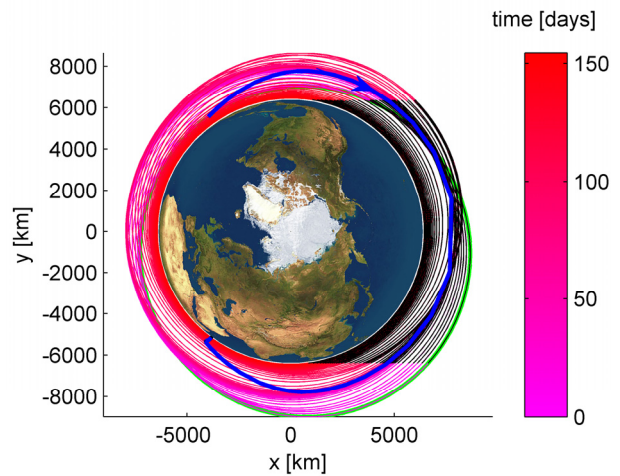
Fig. 5: Librational orbit evolution ($\omega_{s/c} - \lambda_{Sun} = 128.7$ deg) with SRP and drag in an Earth centred reference frame. The colour bar indicates the elapsed time in days.

For an orbit release closer to $\omega_{s/c} - \lambda_{Sun} = \dfrac{\pi}{2}$ the SpaceChip evolution follows a *rotational* orbit in the phase-space, that is $\omega_{s/c} - \lambda_{Sun}$ continues to decrease, as shown with the cyan line in Fig. 6. Such orbits are less suitable for a distributed study of the Earth's upper atmosphere because in some arcs of the trajectory evolution, the SpaceChip perigee orbit is in shadow (highlighted with the black line in Fig. 6). During this period sensing operations and data communication to Earth or to the relay carrier spacecraft will be highly restricted due to power limitations on the device. This is also visible from the representation in an Earth centred reference frame, with its *x*-axis rotating with the Sun-line direction (see Fig. 7). The angular displacement of SpaceChips release (initial condition points on the red line in Fig. 6) determines whether the following orbit evolution will be librational or rotational.
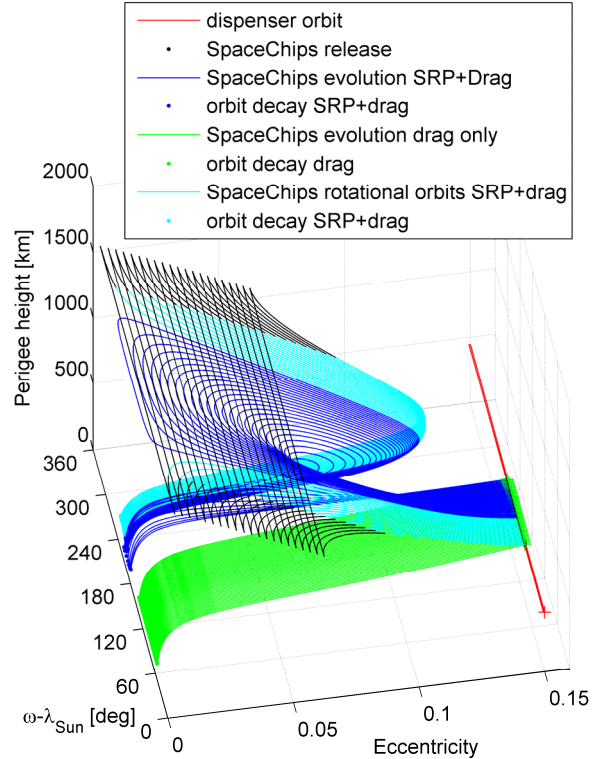
Fig. 6: SpaceChip rotational orbits (cyan line). For these orbits the perigee can be in Earth shadow as highlighted with the black line.

Fig. 7: Rotational orbit evolution ($\omega_{s/c} - \lambda_{Sun} = 125.5$ deg) with SRP and drag in an Earth centred reference frame. The colour bar indicates the elapsed time in days.

Fig. 8 and Fig. 9 represent the atmosphere coverage of the overall mission in terms of perigee and apogee heights (blue line). The exploitation of SRP allows coverage of a more extended region of the atmosphere from the device release (black point) until the final

decay (when the perigee height decreases below 50 km). The swarm will explore an extended region of the ionosphere and the exosphere collecting distributed measurements.

The SpaceChips would evolve towards a fast decay if only drag were influencing their motion (green line in Fig. 8–Fig. 10). This illustrates the importance of the use of SRP to deliver a useful mission life for such small devices with a high area-to-mass ratio. However, the effect of drag can also be exploited to obtain a fast decay of such 'smart dust' devices in the terminal phase of the mission, ensuring their end-of-life disposal and avoiding the creation of long-lived space debris from swarm of devices.

Fig. 10 shows the evolution of semi-major axis. If SRP is exploited (blue line) the orbit energy is maintained almost constant for the first part of the orbit evolution (precisely, the energy slightly increases and then decreases during the librational arc, due to eclipses); in the last phase, instead, the non-conservative effects of atmospheric drag dominates.
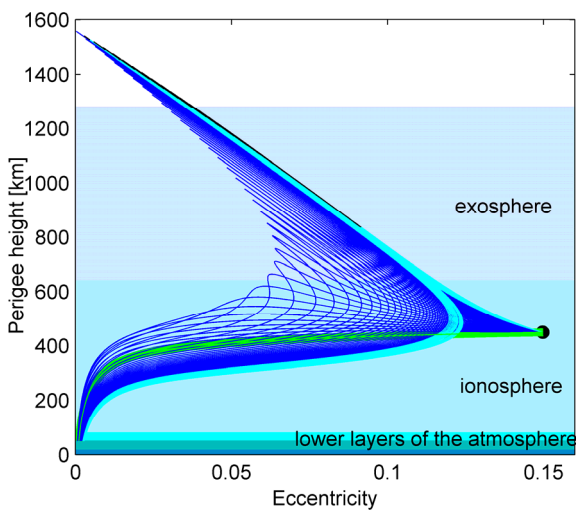
Fig. 8: Perigee height covered for the overall mission as a function of eccentricity. SpaceChip evolution under the effect of SRP and drag (blue line) and drag only (green line). The rotational orbits (SRP and drag) are shown in the cyan line and the arc in which the perigee is in eclipse is highlighted with a black line.
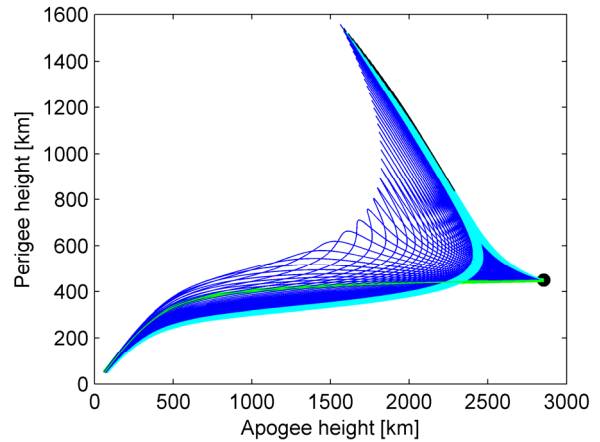
Fig. 9: Perigee and apogee height covered over the mission.
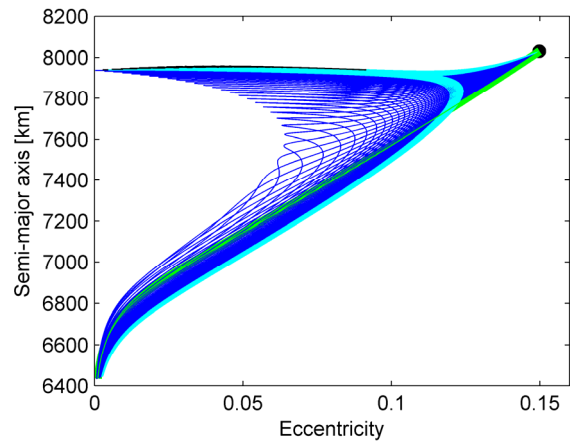
Fig. 10: Evolution of the semi-major axis as function of the eccentricity.

The long-term evolution of the SpaceChip swarms can be also represented in the eccentricity$-\omega_{s/c}-\lambda_{Sun}$ polar reference frame, as in Fig. 11. The dispenser orbit describes a circle over one year (this corresponds to many orbits around the Earth and one revolution of the Earth around the Sun); through this representation it is easy to identify the angular displacement of the dispenser's orbit pericentre at the moment of the SpaceChip release (i.e., second quadrant). The long-term evolution under SRP and drag is indicated with the blue line and the cyan line (rotational orbits, with perigee in shadow highlighted with the black arc), while the evolution subject to drag only is represented with the green line. A different trajectory is generated from each one of the black dots and finally it evolves towards the end-of-life decay at the origin of the graph (green and blue dots).
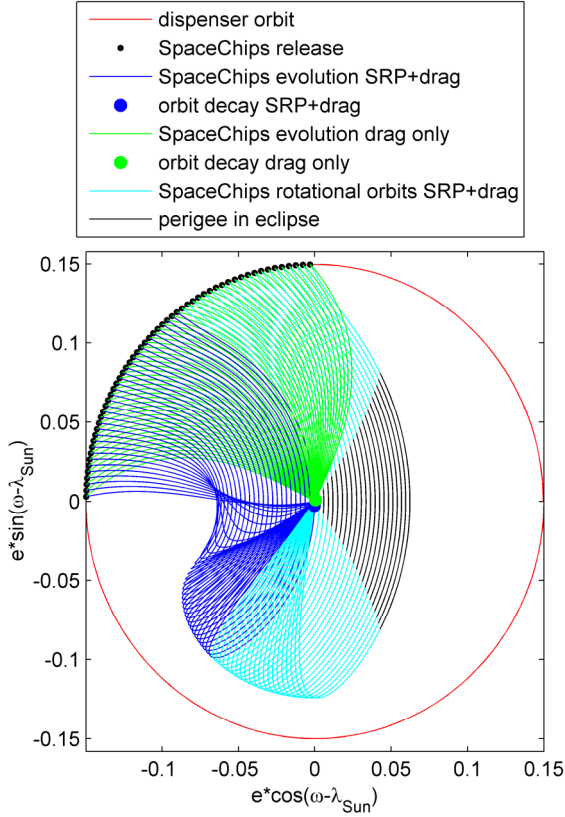
Fig. 11: SpaceChip swarm evolution in eccentricity–$\left(\omega - \lambda_{\text{Sun}}\right)$ polar reference frame.

Importantly, the effect of SRP causes a significant increase in the orbit lifetime with respect to the drag-only case, as shown in Fig. 12, as a function of the angular displacement at release. The orientation of the orbit apse-line relative to the Earth's shadow leads to a gain in orbit energy to balance the dissipation due to air drag, as evidenced by the librating trajectory in the orbital element space (Fig. 4). For this mission the maximum SpaceChip lifetime can be obtained from the condition $\omega_{\text{s/c}} - \lambda_{\text{Sun}} = 151.7 \deg$.
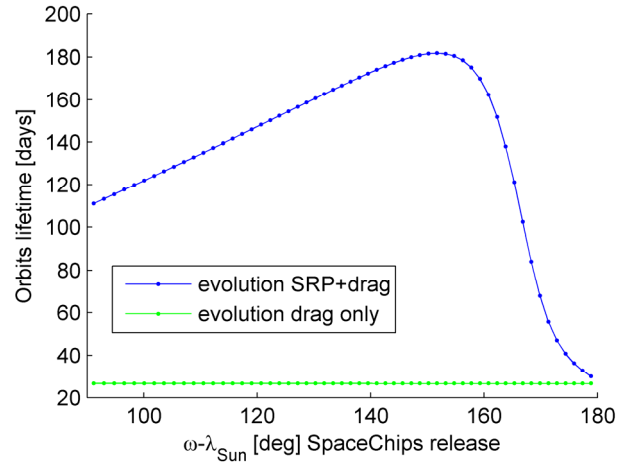
Fig. 12: Orbit lifetime as function of the angular position of SpaceChip release under the effect of SRP and drag (blue line) and drag only (green line).

IV.III. Mission with higher swarm lifetime

The orbit of the carrier spacecraft can be selected in order to ensure a longer lifetime of the SpaceChips after release. Fig. 13 contains the phase-space representation of a more extended mission. The dispenser orbit (red line) is characterised by initial eccentricity of 0.117 and perigee height of 1007.9 km. When transiting on orbits with $\pi/2 < \omega_{\text{s/c}} - \lambda_{\text{Sun}} < \pi$, the conventional spacecraft (Table 2) releases a number of SpaceChips.

Also in this case the SpaceChip evolution is characterised by oscillations in eccentricity and perigee altitude. If the release condition is close to $\omega_{\text{s/c}} - \lambda_{\text{Sun}} = \pi$ the SpaceChip will perform more than one librational loop around the equilibrium condition (branch C of the solution surface in Fig. 2). The spacecraft describes a spiral in the orbital element phase-space. The orbit perigee oscillates around the Sun-line while the orbit stretches and contracts due to the oscillation both in eccentricity and semi-major axis (see the blue line representing the evolution of the orbit pericentre in Fig. 14). Due to the effect of drag, a constant decaying motion is superimposed on the librational motion. This is clearly visible in Fig. 13 and Fig. 15. The effect of drag is almost negligible over the major part of the librational loop and becomes predominant when the perigee reaches its local minimum; in this region the spacecraft experiences a rapid drop in orbit energy, therefore the following librational loop will reach a lower value of the maximum orbit perigee height. The perigee oscillation due to SRP is damped by the presence of drag.

When the SpaceChip orbit design has more then one librational loop in the phase space, the orbit lifetime is consistently higher. This can be seen in Fig. 16 that represents the orbit lifetime (from orbit injection up to

decay below a perigee altitude of 50 km) as a function of the angular displacement of release from the carrier spacecraft. When $\omega_{s/c} - \lambda_{Sun}$ is close to π the orbit lifetime can be up to 20 years.

In the case that the eccentricity of the carrier spacecraft is also left as a mission design parameter (fixing a semi-major axis of 8364.8 km) the orbit lifetime of the 'smart dust' devices is shown in Fig. 17. Each combination of eccentricity and $\omega_{s/c} - \lambda_{Sun}$ corresponds to a different initial condition for the SpaceChip release and its following evolution. Therefore, the lifetime of long-lived orbits can be extended exploiting SRP, and indeed selected depending on the release conditions. Note that the maximum value of lifetime at the centre of the graph in Fig. 17 corresponds to the solution of Eq. 15 (branch C of the solution surface in Fig. 2).

Fig. 14: Librational and progressively decaying orbit evolution ($\omega_{s/c} - \lambda_{Sun} = 128.7$ deg) with SRP and drag in an Earth centred reference frame. The colour bar indicates the elapsed time in days.

Fig. 13: SpaceChip swarm evolution in the phase-space. The dispenser spacecraft follows the red orbit; the long-term evolution of the released chips under the effect of SRP and drag is represented by the blue line. The evolution under the effect of drag only is represented with the green line.
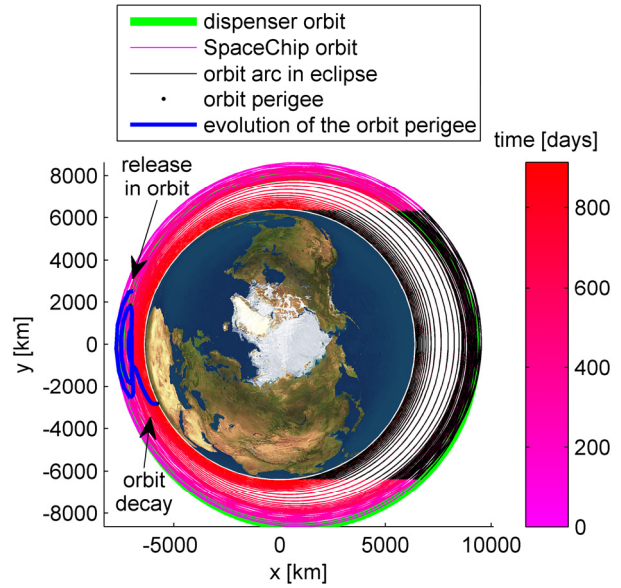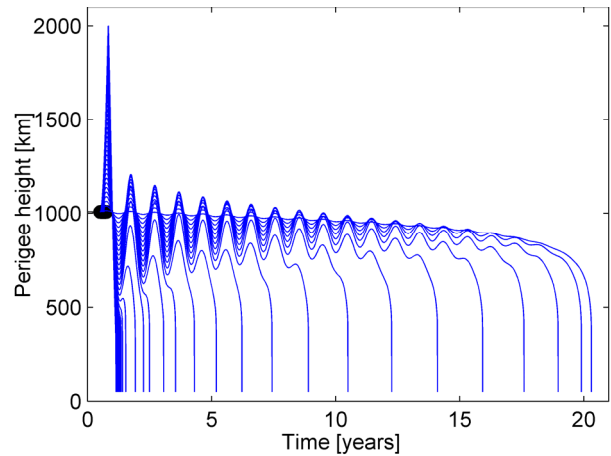

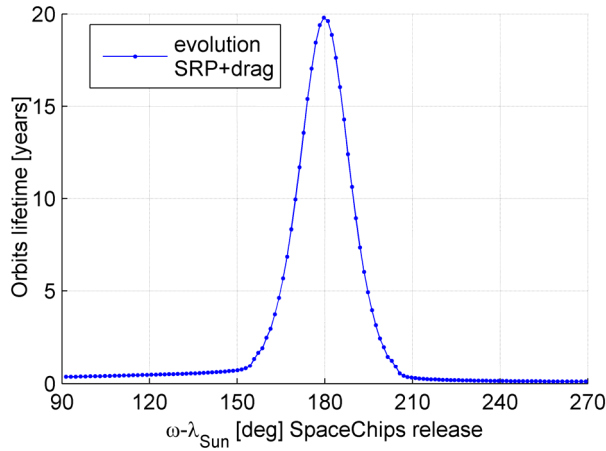Fig. 15: Evolution of the perigee height in time.

Fig. 16 Orbit lifetime as function of the angular position of SpaceChips release.
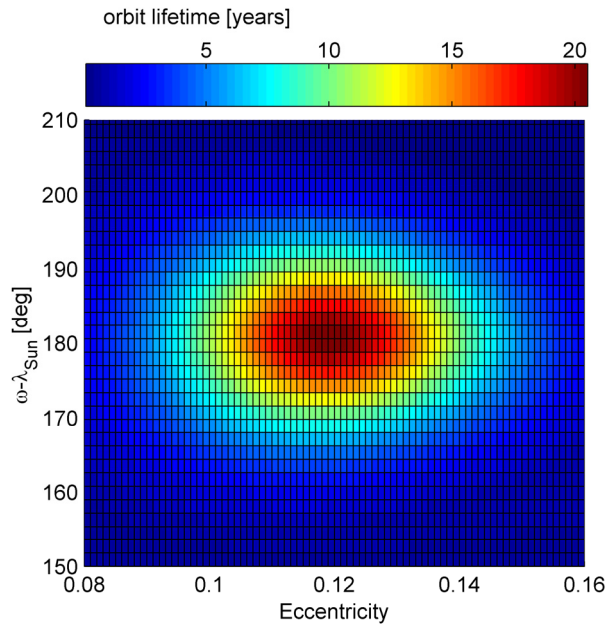

Fig. 17 Orbit lifetime as function of the angular position and eccentricity of SpaceChips release.

The range of altitudes covered in the atmosphere are comparable to the altitudes of the mission in Section IV.II, as can be seen in Fig. 18. The evolution of the SpaceChip swarm is represented with the blue line and the initial orbit of release is shown with the black dot.
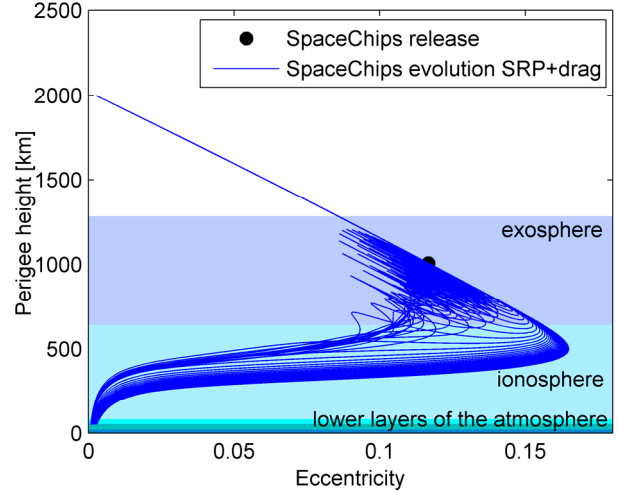

Fig. 18: Perigee height covered over the mission as function of the eccentricity. SpaceChips evolution under the effect of SRP and drag (blue line).

Also in this case the swarm evolution can be represented in the eccentricity$-\left(\omega_{s/c} - \lambda_{Sun}\right)$ polar reference frame, as in Fig. 19. The dispenser orbit describes the red circle over one year, and the release of SpaceChip devices is performed in the second quadrant (for a release in the third quadrant the trajectory would superimpose on the last part of the orbit evolution of the trajectory generated from the black points in the second quadrant).

The long-term evolution under SRP and drag is indicated with the blue line (librational and progressively decaying orbits) and the cyan line (rotational orbits, with perigee in shadow highlighted with the black arc). In this representation it is easy to recognise the trajectories that perform more than one librational loop, for initial conditions close to $\omega_{s/c} - \lambda_{Sun} = \pi$. All the trajectories finally evolve towards the end-of-life decay at the origin of the graph.
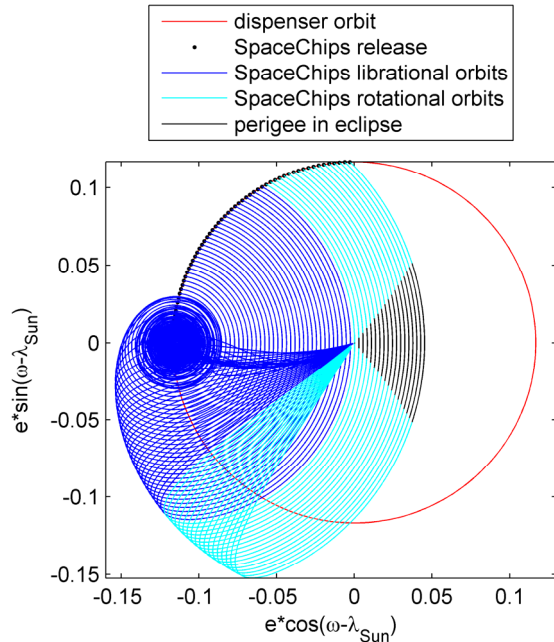
Fig. 19: SpaceChip swarm evolution in eccentricity–$\omega - \lambda_{\mathrm{Sun}}$ polar reference frame.

V. DISCUSSION AND CONCLUSIONS

This paper proposes a mission for the investigation of the upper layers of the Earth's atmosphere which deploys a swarm of SpaceChips from a conventional dispenser spacecraft. Due to the high area-to-mass ratio of these 'smart dust' devices, the coupled effect of atmospheric drag and solar radiation pressure, with asymmetry due to eclipses can be exploited to extend and select the orbit lifetime of such devices and design the disposal of the devices at the end of mission. The swarm covers altitudes between 300 and 1000 km, allowing distributed measurements of the conditions in the ionosphere and exosphere.

It may be inferred that a swarm of SpaceChips could represent a threat for conventional spacecraft orbiting at those altitudes due to the collision hazard [23]. The aim of this paper is to show that the effect of natural perturbations can be exploited to design operational orbits for very small devices and to select initial conditions for their deployment such that a number of distributed measurements can be performed in a defined region of the phase-space. The orbit lifetime can be extended by exploiting SRP, but remains anyway limited by the effect of atmospheric drag. Indeed, the end-of-life of the swarm can be designed, through the passive re-entry in the lower regions of the atmosphere. Moreover, a more active way to control the SpaceChip evolution is currently under study, by changing the reflectivity coefficient of an electro-chromic coating of the spacecraft. This technique could be applied to further limit the domain covered in the phase space, to avoid some forbidden regions where other spacecraft are orbiting [24].

Future work will also address how the effect of the J_2 perturbation affects these long-lived orbits and will possibly will identify other opportunities for swarm missions out of the ecliptic plane.

ACKNOWLEDGMENTS

VI. REFERENCES

[1] Atchison, J. A. and Peck, M. A., "A Passive, Sun-Pointing, Millimeter-Scale Solar Sail," *Acta Astronautica*, Vol. 67, No. 1-2, 2009, pp. 108-121. doi: 10.1016/j.actaastro.2009.12.008

[2] Warneke, B. A. and Pister, K. S. J., "Mems for Distributed Wireless Sensor Networks," *Proceedings of the 9th International Conference on Electronics, Circuits and Systems*, Vol. 1, 2002, pp. 291-294.

[3] Warneke, B., Last, M., Liebowitz, B. and Pister, K. S. J., "Smart Dust: Communicating with a Cubic-Millimeter Computer," *Computer*, Vol. 34, No. 1, 2001, pp. 44-51.

[4] Vladimirova, T., Xiaofeng, W. and Bridges, C. P., "Development of a Satellite Sensor Network for Future Space Missions," *Proceedings of the Aerospace Conference, 2008 IEEE*, 2008, pp. 1-10.

[5] Barnhart, D. J., Vladimirova, T. and Sweeting, M. N., "Very-Small-Satellite Design for Distributed Space Missions," *Journal of Spacecraft and Rockets*, Vol. 44, No. 6, 2007, pp. 1294-1306. doi: 10.2514/1.28678

[6] Miller, L. M., "Mems for Space Applications," *Symposium on Design, Test and Microfabrication of MEMS/MOEMS - Review Paper*, Paris, France, 1999, pp. 1-11.

[7] Janson, S. W., "Silicon Satellites: Picosats Nanonats, and Microsats," *Proceedings of the International Conference on Integrated Micro/Nanotechnology for Space Applications*, The Aerospace Press, Houston, Texas, 1995.

[8] Shapiro, I. I., Jones, H. M. and Perkins, C. W., "Orbital Properties of the West Ford Dipole Belt," *Proceedings of the IEEE*, Vol. 52, No. 5, 1964, pp. 469-518.

[9] Petschek, H. E., Rayburn, C., Sheldon, R., Vickers, J., Bellino, M., Bevis, G. and Spence, H. E., *The Kilo-Satellite Constellation Concept*, Science Closure and Enabling Technologies for Constellation Class Missions, V.A.a.P. Panetta, University of California, 1998, pp. 51-57.

[10] Colombo, C. and McInnes, C., "Orbital Dynamics of Earth-Orbiting 'Smart Dust' Spacecraft under the Effects of Solar Radiation Pressure and Aerodynamic Drag," *AIAA/AAS Astrodynamics Specialist Conference 2010*, Toronto, Canada, 2010. AIAA 2010-7656.

[11] Fortescue, P., Stark, J. and Swinerd, G. (eds.), Spacecraft System Engineering, Third Edition ed. Wiley, Chichester, 2003.

[12] McInnes, C. R., Macdonald, M., Angelopolous, V. and Alexander, D., "Geosail: Exploring the Geomagnetic Tail Using a Small Solar Sail," *Journal of Spacecraft and Rockets*, Vol. 38, No. 4, 2001, pp. 622-629.

[13] Oyama, T., Yamakawa, H. and Omura, Y., "Orbital Dynamics of Solar Sails for Geomagnetic Tail Exploration," *Journal of Guidance, Control and Dynamics*, Vol. 45, No. 2, 2008, pp. 316-323. doi: 10.2514/1.31274

[14] King-Hele, D., *Theory of Satellite Orbits in an Atmosphere*, Butterworths, London, 1964.

[15] Vallado, D. A., *Fundamentals of Astrodynamics and Applications*, Third Edition, Space Technology Library, New York, 2007.

[16] Blitzer, L., "Handbook of Orbital Perturbationss," University of Arizona, 1970.

[17] Abramowitz, M. and Stegun, I. A., *Bessel Functions of Integer Order*, Handbook of Mathematical Functions, 1965, Ch. 9.

[18] Coleman, T. F. and Li, Y., "On the Convergence of Interior-Reflective Newton Methods for Nonlinear Minimization Subject to Bounds," *Mathematical Programming*, Vol. 67, No. 1, 1994, pp. 189-224.

[19] Coleman, T. F. and Li, Y., "An Interior Trust Region Approach for Nonlinear Minimization Subject to Bounds," *SIAM Journal on Optimization*, Vol. 6, No. 2, 1996, pp. 418-445.

[20] Hamilton, D. P. and Krivov, A. V., "Circumplanetary Dust Dynamics: Effects of Solar Gravity, Radiation Pressure, Planetary Oblateness, and Electromagnetism," *Icarus*, Vol. 123, No. 2, 1996, pp. 503-523. doi: 10.1006/icar.1996.0175

[21] Kawaguchi, J. i., Mimasu, Y., Mori, O., Funase, R., Yamamoto, T. and Tsuda, Y., "Ikaros - Ready for Lift-Off as the World's First Solar Sail Demonstration in Interplanetary Space," *Proceedings of the 60th International Astronautical Congress, IAC 2009*, Daejeon, Korea, 2009. IAC-09-D1.1.3.

[22] Dormand, J. R. and Prince, P. J., "A Family of Embedded Runge-Kutta Formulae," *Journal of computational and applied mathematics*, Vol. 6, No. 1, 1980, pp. 19-26.

[23] Rossi, A. and Valsecchi, G., "Collision Risk against Space Debris in Earth Orbits," *Celestial Mechanics and Dynamical Astronomy*, Vol. 95, No. 1, 2006, pp. 345-356. doi: 10.1007/s10569-006-9028-7

[24] Lücking, C. M., Colombo, C. and McInnes, C., "Orbit Control of High Ara-to-Mass Ratio Spacecraft Using Electrochromic Coating," *Proceedings of the 61st International Astronalutical Congress*, Prague, 2010. IAC-10-C1.2.7.